Anomalous, quasilinear, and percolative regimes for magnetic-field-line transport in axially symmetric turbulence

G. Zimbardo, P. Veltri, and P. Pommois

Dipartimento di Fisica, Università della Calabria, I-87030 Arcavacata di Rende, Italy
and Istituto Nazionale di Fisica della Materia, Unità di Cosenza, I-87030 Arcavacata di Rende, Italy

We studied a magnetic turbulence axisymmetric around the unperturbed magnetic field for cases having different ratios $l_\parallel/l_\perp$. We find, in addition to the fact that a higher fluctuation level $\delta B/B_0$ makes the system more stochastic, that by increasing the ratio $l_\parallel/l_\perp$ at fixed $\delta B/B_0$, the stochasticity increases. It appears that the different transport regimes can be organized in terms of the Kubo number $R = (\delta B/B_0)(l_\parallel/l_\perp)$. The simulation results are compared with the two analytical limits, that is the percolative limit and the quasilinear limit. When $R \ll 1$ weak chaos, closed magnetic surfaces, and anomalous transport regimes are found. When $R \approx 1$ the diffusion regime is Gaussian, and the quasilinear scaling of the diffusion coefficient $D_\perp \sim (\delta B/B_0)^2$ is recovered. Finally, for $R \gg 1$ the percolation scaling of the diffusion coefficient $D_\perp \sim (\delta B/B_0)^{0.7}$ is obtained.

PACS number(s): 52.25.Fi, 02.50.Ey, 95.30.Qd, 05.45.−a

I. INTRODUCTION

The transport of heat and particles in magnetized plasmas depends on the electromagnetic turbulence in the plasma itself, as the electromagnetic fluctuations induce ''random'' motions in the directions perpendicular to the average magnetic field. For low frequency magnetic turbulence and strong background magnetic field $\mathbf{B}_0$, the particles approximately follow the magnetic field lines. The quantitative description of magnetic field line transport represents a long standing problem, since different transport regimes can be obtained, depending on the fluctuation level (weak or strong), on the anisotropy of magnetic turbulence, described by the values of the turbulence correlation lengths, on the Fourier spectral representation, and on the assumed dimensionality [i.e., two dimensions (2D) or 3D] of the magnetic fluctuations [1–6]. We assume an unperturbed field $\mathbf{B}_0 = B_0 \hat{\mathbf{e}}_z$ and magnetic fluctuations $\delta\mathbf{B}(\mathbf{r})$ depending on the three spatial coordinates, but frozen in time. The latter assumption corresponds to considering particle velocities larger than the typical magnetic wave velocity, e.g., Alfvén velocity. Note that field line motion in such fields is formally equivalent to the problem of passive tracer transport in a two-dimensional, time dependent velocity field [7,8], so that the main results obtained here can be applied to the problem of transport in fluid turbulence, too.

In this paper, we would like to concentrate our attention on the effect of different correlation lengths $l_\parallel$ and $l_\perp$ in the directions parallel and perpendicular to the mean magnetic field $\mathbf{B}_0$, respectively, that is, on the influence of anisotropy in turbulence with axial symmetry. Indeed, in many physical systems the magnetic turbulence is not spherically symmetric. Axially symmetric turbulence can develop in a plasma as a result of a background magnetic field [9–11], or as a consequence of the geometrical features of a plasma device: in a toroidal configuration, for instance, the correlation length along the toroidal direction is usually much larger than those in the two other directions [12,13]. Also, magnetic turbulence with $l_\parallel \gg l_\perp$ is often assumed as an approximate model for the solar wind [9,6] as well as the interstellar [14] mag-

netohydrodynamic turbulence.

For axially symmetric turbulence, the Fourier spectral amplitude $\delta B(\mathbf{k})$ can be represented as

$$\delta B(\mathbf{k}) \propto \frac{1}{(k_\perp^2 l_\perp^2 + k_\parallel^2 l_\parallel^2)^{\gamma/4 + 1/2}}, \qquad (1)$$

where $\mathbf{k}$ is the wave vector, $k_\perp$ ($k_\parallel$) is the projection of $\mathbf{k}$ in the plane perpendicular (in the direction parallel) to $\mathbf{B}_0$, and γ is the spectral index. Let us introduce a cut off of the spectrum at constant amplitude $\delta B(\mathbf{k})$. Then, for $l_\parallel \gg l_\perp$ the wavevectors are squeezed in the plane perpendicular to $\mathbf{B}_0$, forming a pancake (or crêpe) in the $\mathbf{k}$ space. In such a case, the magnetic turbulence is termed quasi-2D [1,4], the 2D case being obtained by taking the limit $l_\parallel/l_\perp \to \infty$ (and keeping only the Alfvénic polarization for MHD turbulence, see later). Conversely, for $l_\parallel \ll l_\perp$ the wave vectors are elongated along $\mathbf{B}_0$, forming a cigar (or ''spaghetto'') in $\mathbf{k}$ space. In such a case, the domain of magnetic turbulence is quasi-1D, and this magnetic turbulence is termed slab model. Clearly, when $l_\parallel = l_\perp$ the turbulence is spherically symmetric. We also note that if the turbulence is not axially symmetric, as it is in the cases considered here, it is necessary to use three correlation lengths, say l_x, l_y, and l_z, in the expression of the Fourier amplitudes, Eq. (1). This case is of interest in many astrophysical plasmas, like the MHD turbulence in the solar wind and the magnetic fluctuations in the Earth's magnetopause [15–19]. In particular, transport of magnetic field lines in the case of anisotropy in the plane perpendicular to $\mathbf{B}_0$, that is when $l_x \gg l_y$, has been considered by Pommois *et al.* [11].

Several issues need to be taken into account when considering magnetic field line transport in anisotropic turbulence. In the case of weak turbulence, that is when the level of fluctuation $\delta B/B_0$ is low, one has the quasilinear regime, in which the magnetic diffusion coefficient is $D \sim (\delta B/B_0)^2 l_\parallel$ [20–25]. It was shown by Kadomtsev and Pogutse [1] that the quasilinear regime is more properly obtained when the dimensionless parameter $R = (\delta B/B_0)(l_\parallel/l_\perp)$, is very small, $R \ll 1$. In the opposite limit, $R \gg 1$, Kadomtsev and Pogutse

showed that the percolation theory would be required (see also Galeev and Zelenyi [26]). Actually, $R=(\delta B/B_0)(l_\parallel/l_\perp)$ turns out to be the Kubo number for the stochastic system under consideration. The Kubo number R was originally defined as a parameter measuring the strength of perturbations in a stochastic Liouville equation [27]. For fluid turbulence the Kubo number is given by the product of the (rms) fluctuating velocity times its correlation time, divided by the correlation length. Since for field line transport in frozen magnetic turbulence time is to be changed for a coordinate along the unperturbed magnetic field, the above expression of R is obtained. The smallness of the Kubo number allows us to use a perturbative treatment [27]. Also, for times much longer than the correlation time, a Markovian master equation can be obtained from a Liouville equation [27,28] when $R\ll 1$.

Recently, Isichenko [4] derived the scaling of the diffusion coefficient with the level of fluctuations in the percolation limit, $R\gg 1$, obtaining $D\sim l_\perp(l_\perp/l_\parallel)^{3/10}(\delta B/B_0)^{7/10}$ in the case of a monoscale turbulence, i.e., when the fluctuation spectrum is peaked on one frequency. The percolation scaling has been confirmed numerically, with some uncertainty by Ottaviani who used a 64 wave modes model [5] and, more precisely, by Reuss and Misguisch who used a 7168 wave modes [29]. Very recently, the percolation scaling, slightly modified from 0.7 to 0.64, was obtained with a decorrelation path method by Vlad *et al.* [8]. Besides such analytical limits of the Kubo number, it would be interesting to quantify the transport properties for arbitrary values of R, as well as for strong fluctuation levels, $\delta B/B_0\sim 1$, as it is found in many space and astrophysical plasmas. In such cases it is necessary to make use of numerical simulations of field line transport in a turbulent magnetic field. Such a task has been undertaken by several authors [30–36]. In particular, Refs. [30–32] show that in isotropic turbulence (that is when $l_\parallel=l_\perp\equiv l$), at low fluctuation levels, $\delta B/B_0\lesssim 0.2$, anomalous, i.e., superdiffusive and subdiffusive regimes can be found. These regimes are characterized by a mean square deviation $\langle\Delta x^2\rangle$ which grows as

$$\langle\Delta x^2\rangle=2D\,s^\alpha, \tag{2}$$

where s is the field line length, D is the ''diffusion coefficient,'' and $\alpha\neq 1$ is the anomalous diffusion exponent [37–44]. We warn the reader that in this paper anomalous diffusion means the departure from the Gaussian value $\alpha=1$, contrary to most of plasma physics literature where anomalous diffusion is meant for non-collisionally induced transport. While normal, Gaussian diffusion corresponds to $\alpha=1$, subdiffusion (superdiffusion) is described by $\alpha<1$ ($\alpha>1$). Also, superdiffusion is interpreted in terms of a Lévy random walk [38–43]. Such anomalous transport behavior are found when the fluctuation level is low, that is when most magnetic surfaces are closed, i.e., form KAM tori, and a part of field lines move in the stochastic layer. In between KAM tori and ballistic trajectories a Cantori layer is found, which can give rise to temporary trapping of field lines (yielding $\alpha<1$) and to long Lévy flights (yielding $\alpha>1$) [11,30–32,39–42,45]. The Lévy random walk is made up of jumps whose lengths have a power distribution for long jumps. Increasing the level of fluctuations a regime of global

stochasticity is reached, so that the KAM tori are destroyed, and normal diffusion ($\alpha=1$) is attained. This behavior is common to many chaotic systems which exhibit Cantori structures, and has been found in a variety of different physical systems [42,44]. Therefore, for spatially periodic systems to which the KAM theorem applies, anomalous regimes are possible.

Summarizing, we can see that different transport regimes may be found depending on the fluctuation level $\delta B/B_0$ and on the ratio of correlation lengths $l_\parallel/l_\perp$, that is on the anisotropy of magnetic turbulence. In order to understand when there is the transition from one regime to another, we will consider a numerical simulation of magnetic field line transport where $\delta B/B_0$ and $l_\parallel/l_\perp$ can be varied smoothly, and which is presented in the next section.

We find, in addition to the fact that a higher fluctuation level $\delta B/B_0$ makes the system more stochastic, that by increasing the ratio $l_\parallel/l_\perp$ at fixed $\delta B/B_0$, the stochasticity increases. It appears that the different transport regimes can be organized in terms of the Kubo number $R=(\delta B/B_0)(l_\parallel/l_\perp)$. When $R\ll 1$ weak chaos, closed magnetic surfaces, and anomalous transport regimes are found. When $R\approx 1$ the diffusion regime is Gaussian, and the quasilinear scaling of the diffusion coefficient $D_\perp\sim(\delta B/B_0)^2$ is recovered. Finally, for $R\gg 1$ the percolation scaling of the diffusion coefficient $D_\perp\sim(\delta B/B_0)^{0.7}$ is obtained.

In Sec. II we present the numerical model, with special emphasis on the treatment of the anisotropy of turbulence. In Sec. III we present the numerical results, showing the Poincaré sections, the diffusion coefficients and the anomalous diffusion exponents, as well as the kurtosis. It is also shown how the results can be organized in terms of the Kubo number R. In Sec. IV a discussion of our results and the conclusions are given.

II. NUMERICAL MODEL

The magnetic field lines are tangent to the magnetic field $\mathbf{B}(\mathbf{r})$ at a generic point $\mathbf{r}$, thus the field line equations are obtained as

$$\frac{d\mathbf{r}}{ds}=\frac{\mathbf{B}(\mathbf{r})}{|\mathbf{B}(\mathbf{r})|}, \tag{3}$$

where the field line length s is used as an integration parameter. Equation (3) is a nonlinear stochastic ordinary differential equations. We set up a numerical realization of $\mathbf{B}(\mathbf{r})$ in the following way: the magnetic field is taken to be the sum of a background field given by $\mathbf{B}_0=B_0\mathbf{e}_z$ and of static magnetic perturbations $\delta\mathbf{B}(\mathbf{r})$.

The magnetic fluctuations $\delta\mathbf{B}(\mathbf{r})$, are given by

$$\delta\mathbf{B}(\mathbf{r})=\sum_{\mathbf{k},\sigma}\delta B(\mathbf{k})\mathbf{e}^{(\sigma)}(\mathbf{k})\exp i[\mathbf{k}\cdot\mathbf{r}+\phi_\mathbf{k}^{(\sigma)}], \tag{4}$$

where $\mathbf{e}^{(\sigma)}(\mathbf{k})$ are the polarization unit vectors, $\phi_\mathbf{k}^{(\sigma)}$ are random phases, and $\delta B(\mathbf{k})$ is the amplitude of the mode with wave vector $\mathbf{k}$ given by Eq. (1). Such a Fourier amplitude represents a power-law spectrum, and is similar to what is used in Refs. [30,32,11]. We have the following unit vectors for the two polarizations:
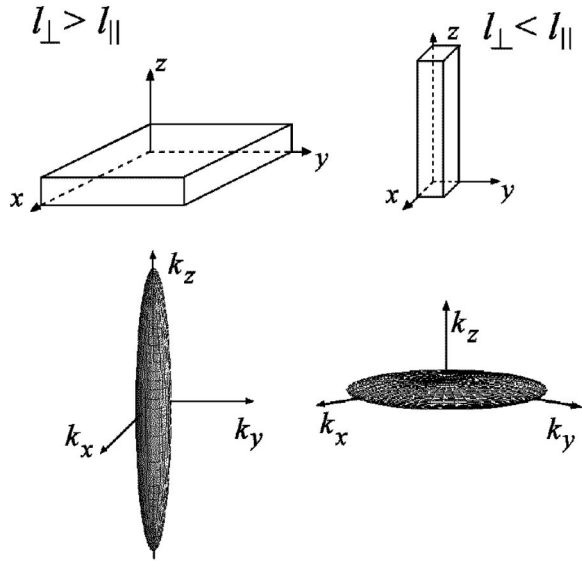
FIG. 1. Simulation box (upper figures) and **k** space (lower figures) representation for two different configurations of the correlations lengths (Slablike model: left hand side figures, 2D-like model: right hand side figures).

$$\mathbf{e}^{(1)}(\mathbf{k}) = i\frac{\mathbf{k} \times \mathbf{B}_0}{|\mathbf{k} \times \mathbf{B}_0|}, \quad \mathbf{e}^{(2)}(\mathbf{k}) = i\frac{\mathbf{k}}{|\mathbf{k}|} \times \mathbf{e}^{(1)}(\mathbf{k}), \quad (5)$$

where $\mathbf{e}^{(1)}(\mathbf{k})$ represents the Alfvénic polarization and $\mathbf{e}^{(2)}(\mathbf{k})$ the magnetosonic one. The reality of $\delta\mathbf{B}(\mathbf{r})$ is enforced by setting $\delta B^{(\sigma)}(-\mathbf{k}) = \delta B^{(\sigma)}(\mathbf{k})$ and $\phi_{-\mathbf{k}}^{(\sigma)} = -\phi_{\mathbf{k}}^{(\sigma)}$. Here (like in Refs. [30,32,11]), we consider the same parameters for both polarizations, even if different set of correlation lengths, weights and spectral index could be given for the two polarizations.

During the integration of the magnetic field lines [see Eq. (3)], we save computer time by introducing a 3D lattice with $8N_{max}$ points in each direction, on which the magnetic field components are computed exactly. Then, when integrating, the magnetic field is obtained by quadratic interpolation on this grid. We checked that 8 points per minimum wavelength are enough to get satisfactory precision [30,32].

We consider the wave vectors in the following way:

$$\mathbf{k} = 2\pi\left(\frac{n_x}{L_x}, \frac{n_y}{L_y}, \frac{n_z}{L_z}\right), \quad (6)$$

where the harmonic numbers n_i are integers. The periodicity length in each direction is $L_x = L_y = N_{min}l_\perp$ and $L_z = N_{min}l_\parallel$, where N_{min} is the minimum harmonic number (see below), therefore it is proportional to the correlation length in that direction. Thus, the simulation box is a parallelepiped with square basis, and the domain of wavevectors in **k** space is an axially symmetric ellipsoid, see Fig. 1. Indeed, the harmonic numbers have to satisfy

$$N_{min}^2 < n_x^2 + n_y^2 + n_z^2 < N_{max}^2, \quad (7)$$

where N_{max} is the maximum harmonic number, which corresponds to a short wavelength cut off. This is related to the extention of the spectrum and its value is fixed by the available numerical resources. A long wave length cut off is in-

troduced by taking $N_{min} > 1$. Therefore we have a *band* spectrum. In this way we avoid the spurious periodicity effects introduced by the discretization of the **k** space similar to the poor statistical representation of the longest wavelength modes [32]. With this choice, we obtain the longest modes in each direction with wavelengths $\lambda_x = \lambda_y \simeq l_\perp$ and $\lambda_z \simeq l_\parallel$, by setting n_i equal to the smallest integer larger than N_{min}. In other words, the correlation lengths $l_\perp$ and $l_\parallel$ determine the physical features of the modelled magnetic turbulence. Furthermore the number of wave vectors is the same along each axis, even with differents values of $l_\perp$ and $l_\parallel$ [see Eqs. (6) and (7)] [46]. This ensures that a good statistical representation of turbulence is given even for those wave vectors which lay along the ''short'' directions in **k** space (in other words, if the number of the wave vectors along one axis would be merely proportional to the length of the ellipsoid axis, only few wave vectors would be found along the short axis of the ellipsoid, and the discretization of turbulence would lead to the dominance of just a few modes). Indeed, we are going to simulate very strong anisotropies, e.g., $l_\perp \gg l_\parallel$ and $l_\perp \ll l_\parallel$, with the same number of modes which we use for isotropic turbulence. For instance, the so-called quasi-2D turbulence, corresponding to $l_\parallel/l_\perp \gg 1$, will be represented by a fully 3D spectrum, although squeezed to a crêpe in the in **k** space (at variance with other works where the quasi-2D turbulence is represented by a strictly 2D spectrum). This garantees that the continuum spectrum of turbulence is well represented by our discretized spectrum and that we can pass smoothly from one ratio $l_\parallel/l_\perp$ to another. Further, in physical space we have the same number of grid points in all the directions, with density of grid points proportional to the field gradients in each direction. Thus we consider that our numerical representation of turbulence is very well suited to study the effects of varying anisotropy.

The value of N_{max} is set to 14, while $N_{min} = \sqrt{17}$. We set for all the numerical runs $\gamma = 3/2$, which is the value of the spectral index inertial range predicted by Kraichnan [47]. Furthermore, we set for all runs $\min(L_x, L_z) = L$ where L is the unit length to which all lengths in this paper are normalized. [That is, for $l_\parallel/l_\perp > 1$, $L_x = L$ and $L_z = (l_\parallel/l_\perp)L$; for $l_\parallel/l_\perp < 1$, $L_z = L$ and $L_x = L_y = (l_\perp/l_\parallel)L$.]

The desired fluctuation level $\delta B/B_0$ is obtained by normalizing the magnetic fluctuations by setting

$$\frac{\delta B}{B_0} = \sqrt{\frac{\sum_{ijk} \delta B_{ijk}^2}{(8N_{max})^3 B_0^2}}, \quad (8)$$

where the sum is made all over the grid points. Then the numerical simulation will be done for different values of $l_\parallel/l_\perp$ and $\delta B/B_0$, and hence for different values of the Kubo number.

III. NUMERICAL RESULTS

Once a numerical realization of the magnetic field is obtained as described in Sec. II, we integrate the magnetic field line equations (3). We make two kinds of studies. First, in order to get a qualitative overview of transport and of the structure of the magnetic field, we draw the projection on the

TABLE I. Parameters of the different runs of numerical simulations.

Run	$l_\parallel/l_\perp$	$\langle \delta B_z^2\rangle/\langle \delta B_x^2\rangle$
1	100	2.00
2	10	1.93
3	3	1.61
4	1	1.04
5	0.33	0.45
6	0.1	0.16
7	0.01	0.12

plane xy of the intersection of the magnetic field line with a plane at integer values of z/L_z. We will call this projection a Poincaré section. We follow a few field lines (typically, 12 lines) integrating Eq. (3) from $s=0$ to $s=600L_z$. As the field lines are traveling mostly along z then we have in this way a view of the evolution of the transport transversal to the magnetic field. Second, we do an accurate quantitative study by calculating the variances $\langle \Delta x_i^2\rangle$ as a function of s, averaged over 1000 field lines. In both cases the starting point of each field line is taken at $z=0$ and is randomly distributed in the square $0\leqslant x\leqslant L_x$, $0\leqslant y\leqslant L_y$.

The different runs, where the ratio $l_\parallel/l_\perp$ is varying, are described in Table I. Also reported is the ratio $\langle \delta B_z^2\rangle/\langle \delta B_x^2\rangle$, which shows how the magnetic fluctuation energy is distributed along the different directions, for each realization of the fluctuating field (clearly, this ratio equals 1 for $l_\parallel=l_\perp$, for run 4). While the ratio $\langle \delta B_y^2\rangle/\langle \delta B_x^2\rangle$ in the xy plane equals 1 (not reported) because of axial symmetry, $\langle \delta B_z^2\rangle/\langle \delta B_x^2\rangle$ tends to 2 for $l_\parallel/l_\perp\to\infty$, and becomes very small for $l_\parallel/l_\perp\to 0$. The former result is because for very large $l_\parallel/l_\perp$ the wave vectors are squeezed in the xy plane, and each wave vectors has one polarization in the xy plane ($\hat{\mathbf{e}}_1$) and one almost parallel to $\mathbf{B}_0$ ($\hat{\mathbf{e}}_2$), so that δB_z gets twice as much independent contributions as δB_x or δB_y. The latter result is because for very small $l_\parallel/l_\perp$ all the wave vectors are aligned along z, and the polarization vectors $\hat{e}_1$ and $\hat{e}_2$ almost lay in

the xy plane, so that only a small amount of the fluctuating field is along z. (Note that wave modes with $\mathbf{k}$ exactly parallel to $\mathbf{B}_0$, that is with $n_x=n_y=0$, are excluded from our simulation because $\hat{e}_1$ and $\hat{e}_2$ are undetermined; this is not relevant to the magnetic field model due to the high number of wave modes, typically 11 512; in addition, this explains why for run 4, $\langle \delta B_z^2\rangle/\langle \delta B_x^2\rangle=1.04$, rather than 1 as would be expected for exact isotropy.)

A. Poincaré sections

The Poincaré sections for some of the runs are plotted in Figs. 2 and 3. Looking at these plots, it can be seen that, due to the introduction of the longwavelength cut off $N_{\min}=\sqrt{17}$, we do not observe, even for very high anisotropy, effects of periodicity in these figures. Also, transport is rather isotropic in the xy plane, as it should be since $l_x=l_y=l_\perp$. In Fig. 2, the Poincaré sections are plotted for a ratio $l_\parallel/l_\perp$ increasing from left to right (that is $l_\parallel/l_\perp=0.1$, 0.33, and 3, for respectively runs 6, 5, and 3). Two different fluctuation levels $\delta B/B_0$ are plotted in the figure: $\delta B/B_0=0.1$ for the upper panels and $\delta B/B_0=0.3$ for the lower panels, so that the fluctuation level is increasing from top to bottom. The differences between the various runs are striking: for the lower ratio $l_\parallel/l_\perp$ (on the left) we distinguish very well defined magnetic surfaces and magnetic islands, while for the higher ratio $l_\parallel/l_\perp$ (on the right), the magnetic surfaces are completely destroyed even at moderate fluctuation levels. Therefore an increase of the $l_\parallel/l_\perp$, for the same fluctuation level, increases the stochasticity of the system.

As in the isotropic case an increase of $\delta B/B_0$ makes the system more stochastic. However, the value of $\delta B/B_0$ is not the only parameter which determines the stochasticity of the system. Rather, it appears that anisotropy, quantified by $l_\parallel/l_\perp$, has a very strong influence on the stochasticity of magnetic field lines. It is clear from Fig. 2 that stochasticity increases with $l_\parallel/l_\perp$. This in spite of the fact that the magnetic fluctuation energy in the perpendicular direction, described by the ratio $\langle \delta B_z^2\rangle/\langle \delta B_x^2\rangle$ in Table I, decreases when $l_\parallel/l_\perp$ increases. We note here that although a very large
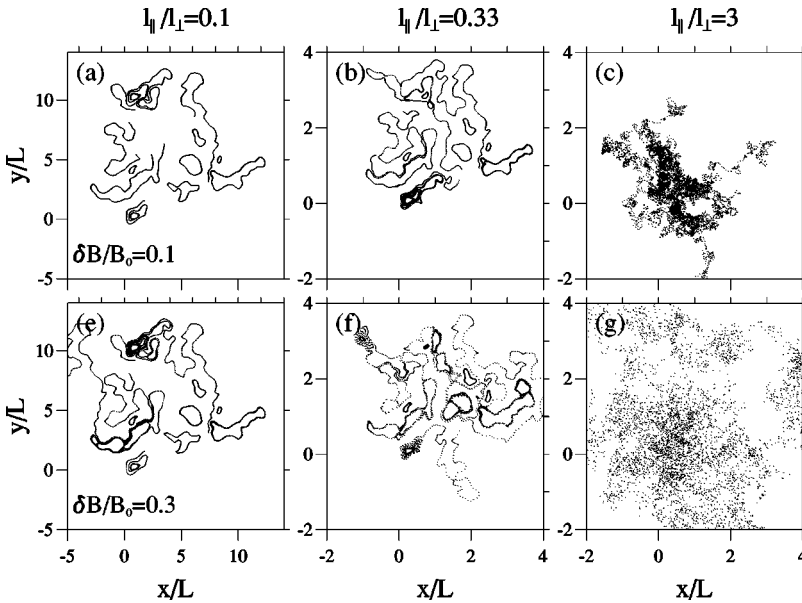
FIG. 2. Poincaré sections at various $\delta B/B_0$ and for different ratio $l_\parallel/l_\perp$. (a)–(c), $\delta B/B_0=0.1$; (e)–(g): $\delta B/B_0=0.3$; (a) and (e): $l_\parallel/l_\perp=0.1$; (b) and (f): $l_\parallel/l_\perp=0.33$; (c) and (g): $l_\parallel/l_\perp=3$.
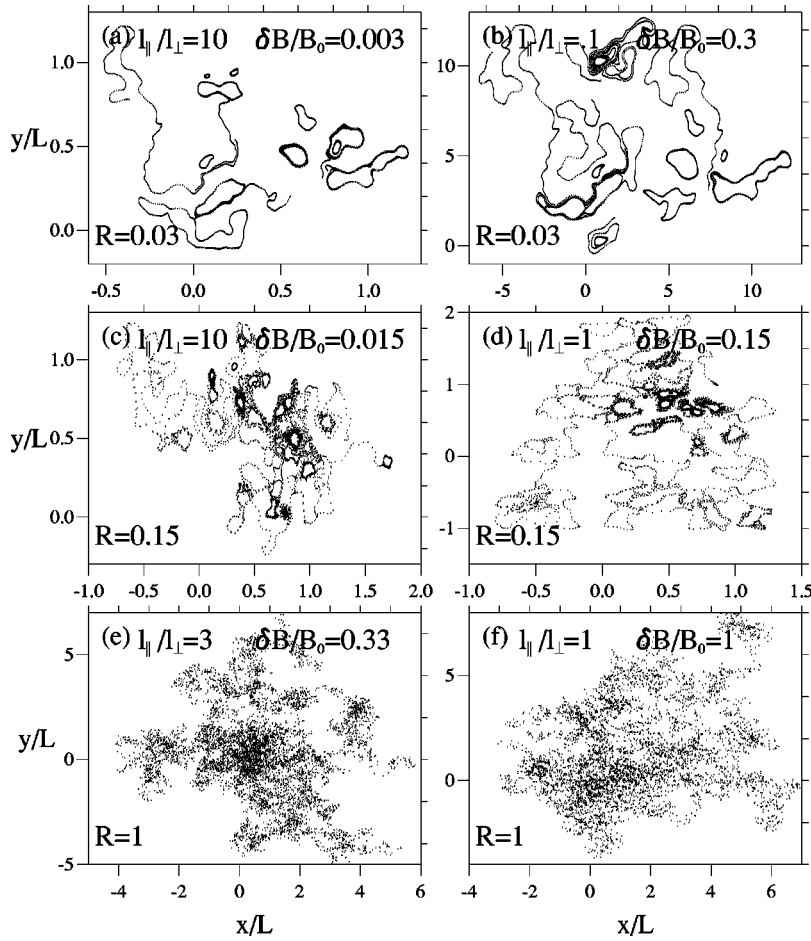
FIG. 3. Poincaré sections for runs with the same value of $R = (\delta B/B_0)(l_\parallel/l_\perp)$, but different fluctuation levels and anisotropy degrees: (a): $\delta B/B_0 = 0.003$ and $l_\parallel/l_\perp = 10$ (run 2, $R = 0.03$); (b): $\delta B/B_0 = 0.3$ and $l_\parallel/l_\perp = 0.1$ (run 6, $R = 0.03$); (c): $\delta B/B_0 = 0.015$ and $l_\parallel/l_\perp = 10$ (run 2, $R = 0.15$); (d): $\delta B/B_0 = 0.15$ and $l_\parallel/l_\perp = 1$ (run 4, $R = 0.15$); (e): $\delta B/B_0 = 0.33$ and $l_\parallel/l_\perp = 3$ (run 3, $R = 1$); (f): $\delta B/B_0 = 1$ and $l_\parallel/l_\perp = 1$ (run 4, $R = 1$).

number of studies has addressed the issue of how the stochasticity level depends on the fluctuation level, this is the first time that the influence of anisotropy on stochasticity is pointed out with a systematic study.

From the inspection of Fig. 2 we can understand that the level of stochasticity depends on a parameter which is made up of the level of fluctuations and the degree of anisotropy. It appears that the Kubo number $R = (\delta B/B_0) l_\parallel / l_\perp$, which originally was defined to measure the effect of stochastic perturbations over one correlation time (see the Introduction), can be such a parameter. To this end, we show in Fig. 3 some Poincaré sections with different $\delta B/B_0$ and $l_\parallel / l_\perp$, but the same value of R: it is apparent that the level of stochasticity is (at least from a visual point of view) the same for a given value of R. In other words the value of R determines the level of chaos, with $R \approx 1$ corresponding to global stochasticity.

The Poincaré sections on the left panels of Fig. 2 (those with $l_\parallel < l_\perp$) suggest a subdiffusive behavior, as it is found also from the study of transport (see later). The very well defined closed curves plotted on the left panels show that the magnetic field lines spiralize around the flux tubes and stay on them for a long time. As $\delta B/B_0$ is increased, the stochastic layer is getting thicker (although still very thin) and this means that the field lines can escape more easily from one flux tube and then be trapped in another. Some other field lines have superdiffusive behavior because they are moving for quite long distances in the stochastic layer, and are subject to long displacements very similar to Lévy flights (see the open trajectories in Fig. 2).

B. Anomalous transport

The different transport regimes, which are suggested by the Poincaré sections, as well as the role of the Kubo number R, can be better caracterized by studying quantitatively the transport properties. In this connection, we integrate Eq. (3) to compute the variances $\langle \Delta x_i^2 \rangle$, where $\Delta x_i = x_i - x_i^{(0)}$ ($i = x,y$), as a function of s (here the field line length s has a role analogous to time). Then we make a fit of $\langle \Delta x_i^2 \rangle$, with the anomalous transport law

$$\langle \Delta x_i^2 \rangle = 2D_i \, s^{\alpha_i} \tag{9}$$

and determine α_i and D_i when s is large enough to attain asymptotic values. The asymptotic behavior is usually obtained for $s = 1000L_z$ or less. Here, the exponent α_i characterizes the random walk law: $\alpha_i = 1$ in the Gaussian diffusive regime, $\alpha_i = 2$ in the ballistic regime; $\alpha_i < 1$ in the case of trapping (subdiffusive regime), and $1 < \alpha_i < 2$ in the case of Lévy random walk (superdiffusive regime) (Refs. [30,40–42,44]). We note that the superdiffusive case when $1 < \alpha_i < 2$ usually corresponds to an alternate succession of short jumps and of long jumps (Lévy flights) between two magnetic flux tubes. To have a good statistics, the above transport expression is fitted to the numerical results obtained with a large number of field lines, tipically 1000.

In Fig. 4, we plotted the anomalous diffusion exponents as a function of $\delta B/B_0$ for a selection of runs. The same behavior found in previous studies [30–32,11] is confirmed: for a given degree of anisotropy, α_i tends to 1 (Gaussian
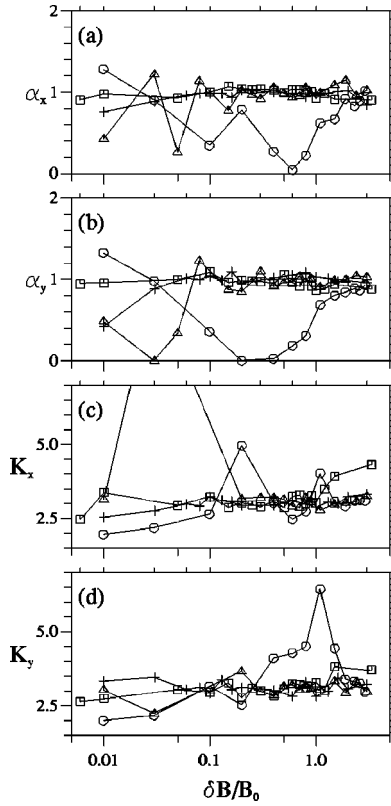
FIG. 4. Anomalous diffusion exponents α_x and α_y versus $\delta B/B_0$ [(a) and (b)]. Kurtosis K_x and K_y versus $\delta B/B_0$ [(c) and (d)]. $l_{\parallel}/l_{\perp} = 100$: squares; $l_{\parallel}/l_{\perp} = 10$: crosses; $l_{\parallel}/l_{\perp} = 1$: triangles; $l_{\parallel}/l_{\perp} = 0.1$: circles.

diffusion) when $\delta B/B_0$ is increased, and α_i is different from 1 for low $\delta B/B_0$. In the latter cases, we find mostly subdiffusion, i.e., $\alpha_x < 1$, $\alpha_y < 1$ (see later). However, the smaller $l_{\parallel}/l_{\perp}$, the higher $\delta B/B_0$ has to be in order to attain $\alpha_i = 1$, see the upper two panels of Fig. 4. This agrees with the fact, discussed above, that global stochasticity is reached for a higher level of fluctuations when $l_{\parallel}/l_{\perp}$ is decreased. We note that $\alpha_i \neq 1$ corresponds to a non Gaussian ''dynamics.'' Indeed, the Lévy random walk is characterized by a distribution of free path lengths which is power law rather than Gaussian [40,41] and which has diverging second order moment. Further, $\alpha_i = 1$ does not always mean Gaussian regime but can be the result of a mix of trapping events and Lévy flights such that normal transport is found [5]. This fact can be evidenced by computing the kurtosis $K_i = \langle \Delta x_i^4 \rangle / \langle \Delta x_i^2 \rangle^2$, which equals 3 for a Gaussian distribution. A kurtosis larger than 3 corresponds to enhanced importance of the tails (as for Lévy stable law distribution), while $K_i < 3$ implies very short tails of the distribution. From the kurtosis in Fig. 4, we have indication of Lévy flights (since $K_i > 3$) for various cases, even with $\alpha_i \approx 1$; then for a particular fluctuation level, that increases with the ratio $l_{\perp}/l_{\parallel}$, the kurtosis is equal to 3, i.e., the bunch of magnetic field lines has a Gaussian distribution, corresponding to normal diffusion.

Note that anomalous diffusion, $\alpha \neq 1$, is mostly found for small values of $l_{\parallel}/l_{\perp}$. We interpret this as the influence of the limited stochasticity (weak chaos) on transport: in the presence of good magnetic surfaces (see Fig. 2) and of KAM tori, many field line are trapped on KAM tori and give a very

low contribution to transport (this contribution goes asymptotically to zero for $s \rightarrow \infty$). Other field lines are in the stochastic layer and move in between the magnetic ''islands'' with long coherent displacements which correspond to the Lévy flight (leading to superdiffusion), and others are on Cantori layers. The latter is a region of broken magnetic surfaces which are adjacent to KAM tori, on which field lines can be trapped for long times and then escape into the stochastic layer. It is typical of Cantori layers to have a fractal structure as well as a hierarchy of trapping times with power law distribution [42–44]. It is the balance between trapping in Cantori and Lévy flight in the stochastic layer that leads either to $\alpha < 1$ (trapping prevails) or to $\alpha > 1$ (Lévy flights prevail) [30]. At the same time, it is well known that anomalous diffusion is found in systems characterized by weak, incomplete chaos [42–44].

On the other hand, increasing the level of stochasticity, i.e., $R = (\delta B/B_0)(l_{\parallel}/l_{\perp})$, the area occupied by KAM tori decreases, the thickness of the stochastic layer increases and, because of the enhanced instability of trajectories, the length of Lévy flights and of trapping times on Cantori both decrease. Thus, in a regime of global stochasticity the field line random walk approaches a Gaussian regime (characterized by finite jump length and jump time) and normal diffusion is recovered.

C. Threshold of the Gaussian diffusion

Let us now investigate what are the conditions to have normal rather than anomalous diffusion. As shown above, the anisotropy in the correlation lengths influences in a consistent way the regime of diffusion. In particular, from Fig. 4, we note that that the value of $\delta B/B_0$ for which the kurtosis becomes close to 3, decreases when increasing the ratio $l_{\parallel}/l_{\perp}$. Also from Fig. 6 of Ref. [11], we note that the stochastic regime is reached for a higher fluctuation level when the anisotropy l_x/l_y is increased, i.e., the threshold for the Gaussian regime is increasing with the ratio l_x/l_y (in Ref. [11] $l_y = l_z$, so that the ratio l_x/l_y mimics $l_{\perp}/l_{\parallel}$). We observed in connection with Fig. 3 and in previous works [46] similar stochasticity levels when the Kubo number $R = (\delta B/B_0)(l_{\parallel}/l_{\perp})$ is the same. Also, the quasilinear regime and the percolation regime are obtained for opposite limiting values of R. For these reasons, we plotted in Fig. 5(a) the value of $(\delta B/B_0)^*$ for which the kurtosis attained 3.0 ± 0.3 (that is the Gaussian value $\pm 10\%$ [31]), versus the anisotropy ratio $l_{\parallel}/l_{\perp}$. We observe an almost inverse linear relation between the ratio $l_{\parallel}/l_{\perp}$ and the threshold for Gaussian regime $(\delta B/B_0)^*$. In other words, $(\delta B/B_0)^* l_{\parallel}/l_{\perp} \simeq$ constant holds.

Then we can define the threshold Kubo number, that is $R^* = (\delta B/B_0)^* l_{\parallel}/l_{\perp}$, at which we reach the Gaussian regime. Therefore, we have anomalous transport regimes for $R < R^*$, and Gaussian diffusion for $R > R^*$. In the Fig. 5(b), we plotted R^* versus the ratio $l_{\parallel}/l_{\perp}$. We can see that R^* has values going from 0.3 to 0.6, so that $R^* \approx 1$ is a reasonable criterion to determine the Gaussian threshold in our simulations. We note that this interpretation of the role of the Kubo number is fully consistent with that obtained from the above analysis of the Poincaré sections.
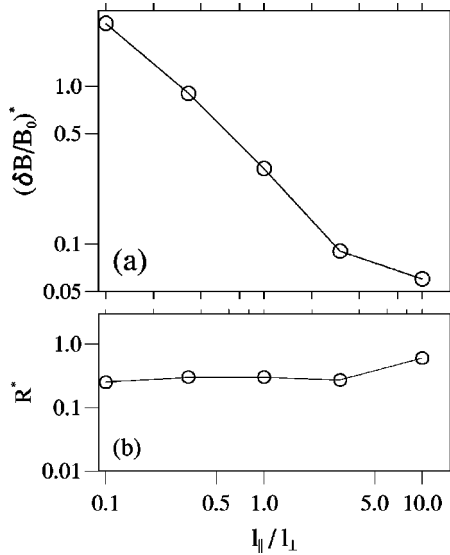
FIG. 5. Minimum value of the fluctuation level $(\delta B/B_0)^*$ at which the kurtosis is between 3.3 and 2.7 (upper panel), and Kubo number R^* (for which the system passes from anomalous regime to Gaussian regime, lower panel) as a function of the ratio $l_\parallel/l_\perp$ for the different runs.

Actually, there are other parameters which influence the threshold of stochasticity, as well. For example, Zimbardo *et al.* [30] showed that with a longer spectral extention, global stochasticity is attained for lower values of the fluctuation level (a well known result, see also Refs. [22,48]). Recently, Pommois *et al.* [32] showed that the shape of the spectrum, that is the balance between the injection zone and the inertial range in the simulated turbulence, also influences the reach of the Gaussian regime. Here we singled out the influence of $l_\parallel/l_\perp$ on the stochasticity and Gaussian threshold, and we leave for future investigations the study of the influence of the other parameters.

D. Scaling of the diffusion coefficients

In Fig. 6, we plotted the diffusion coefficients D_i for the various runs but only when we are in the Gaussian regime. In practice, the cases with $R \ll 1$, which would correspond to the quasilinear diffusion coefficient according to the analytical studies, turn out to be in the anomalous diffusion regime, so that the coefficient D_i of the fit of Eq. (9) does not have the meaning of a standard diffusion coefficient. We note that transport is faster when the ratio $l_\parallel/l_\perp$ is increased, especially for the lower fluctuation levels. Indeed, the scaling of the diffusion coefficient with $\delta B/B_0$ appears to be different for the different degree of anisotropy (compare for instance runs 1 and 4).

In order to make the comparison with the analytical limits, let us introduce the transversal diffusion coefficient $D_\perp$, corresponding to diffusion in the plane perpendicular to $\mathbf{B}_0$. Since we have $\langle \Delta r_\perp^2(s) \rangle = \langle \Delta x^2(s) \rangle + \langle \Delta y^2(s) \rangle$, we obtain directly that $D_\perp = D_x + D_y$. We now consider more closely the scaling of the diffusion coefficients $D_\perp$ with the fluctuation $\delta B/B_0$, that is

$$D_\perp \propto \left(\frac{\delta B}{B_0} \right)^\mu \qquad (10)$$
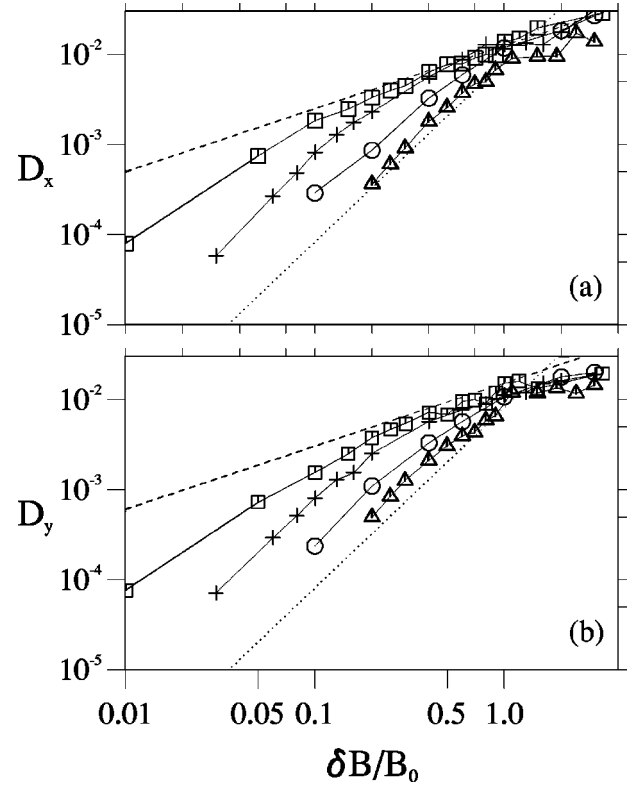
FIG. 6. Diffusion coefficients D_x and D_y versus $\delta B/B_0$ (in Gaussian regime). $l_\parallel/l_\perp = 100$: squares; $l_\parallel/l_\perp = 10$: crosses; $l_\parallel/l_\perp = 3$: circles; $l_\parallel/l_\perp = 1$: triangles. To estimate the scaling of D_i with the fluctuation level, $D_i \propto (\delta B/B_0)^\mu$, we plotted both the quasilinear diffusion scaling with $\mu = 2$ (dotted line) and the percolative diffusion scaling with $\mu = 0.7$ (dashed line).

and compare it with the quasilinear limit and with the percolative limit.

In Fig. 7, $D_\perp$ is plotted for all the runs as a function of the Kubo number R. Several interesting features can be appreciated from this figure. The quasilinear (percolative) scaling of the diffusion coefficient with $\delta B/B_0$ is given by the dotted (dashed) lines (at a fixed anisotropy ratio $l_\parallel/l_\perp$, the scaling of $D_\perp$ with $\delta B/B_0$ is the same as that with R). Since each different symbol in the figure represents a run with given anisotropy, it is easy to see that for $R \lesssim 1$ the $D_\perp$ follow the quasilinear scaling for all the different anisotropy ratios. Also, for $R \gtrsim 10$, the diffusion coefficient scales with R as in the percolative regime. It is possible that the scaling of $D_\perp$ with R would be somewhat slower than the value proposed by Isichenko, $\mu = 0.7$ [4], and in agreement with theorical predictions by Vlad *et al.* [8]. However, our data points are not enough to strictly constrain the value of μ in the percolative regime. From $R \simeq 1$ to $R \simeq 10$, an intermediate scaling appears: although this might look similar to the so-called Bohm scaling, $D_\perp \sim R$, we consider this to be only a transition regime from the quasilinear scaling to the percolation scaling. Moreover, the theorical foundations of the Bohm scaling have been recently questioned by Reuss and Misguich and Vlad *et al.* [29,8].

If we look at the left most part of Fig. 7, we have a confirmation of the fact that the Gaussian diffusion regime is reached when $R \simeq 0.3-0.4$, since the diffusion coefficient
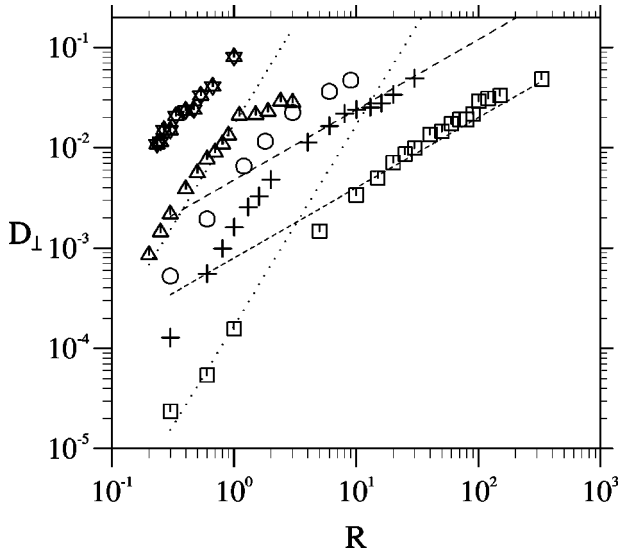
FIG. 7. Anomalous diffusion coefficients $D_\perp$ versus Kubo number R. $l_\parallel/l_\perp = 100$: squares; $l_\parallel/l_\perp = 10$: crosses; $l_\parallel/l_\perp = 3$: circles; $l_\parallel/l_\perp = 1$: triangles; $l_\parallel/l_\perp = 0.33$: stars. We also plotted the quasilinear scaling with $\mu = 2$ (dotted lines), and the percolative scaling with $\mu = 0.7$ (dashed lines).

are not obtained for smaller values of R. Furthermore, we can see that for a given value of R, $D_\perp$ depends strongly on the anisotropy ratio $l_\parallel/l_\perp$, with the larger value of $D_\perp$ obtained for the smaller $l_\parallel/l_\perp$. This result can be easily explained when we write down the quasilinear diffusion coefficient in terms of the Kubo number

$$D_{\rm ql} \simeq \beta_{\rm ql}\left(\frac{\delta B}{B_0}\right)^2 l_\parallel = \beta_{\rm ql}\frac{l_\perp^2}{l_\parallel}R^2. \qquad (11)$$

It is clear that the smaller $l_\parallel/l_\perp$, the larger $D_\perp$; also, inspection of Fig. 7, shows that our data points follow this relation rather well. A fit of the data points in the quasilinear regime to Eq. (11) allows us to determine the proportionality constant $\beta_{\rm ql}$ as $\beta_{\rm ql} \approx 0.015$. In a similar way, in the percolative regime $D_\perp$ is larger for smaller $l_\parallel/l_\perp$, and we can write the Isichenko diffusion coefficient in terms of R:

$$D_{\rm p} \simeq \beta_{\rm p} l_\perp\left(\frac{l_\parallel}{l_\perp}\right)^{0.3}\left(\frac{\delta B}{B_0}\right)^{0.7} = \beta_{\rm p}\frac{l_\perp^2}{l_\parallel}R^{0.7}. \qquad (12)$$

This is the same expression as above, Eq. (11), apart from the dependence on R and the proportionality constant β_p. This relation is approximately followed by $D_\perp$ in the percolative regime, $R \gtrsim 10$, too, and a fit of the data points yields $\beta_{\rm p} \approx 0.06$.

It is important to notice here that although the Kubo number $R = \delta B/B_0 l_\parallel/l_\perp$ is the fundamental parameter which determinates the transport regime, e.g., anomalous, quasilinear, or percolative, yet it is not the only parameter to determine the value of the diffusion coefficient $D_\perp$, as clearly indicated by Fig. 7: the anisotropy ratio $l_\parallel/l_\perp$ also plays an important role (of course, we are limiting such considerations to the parameters which are varied in the present study).

Finally, it is interesting to note that the analytical studies predict a quasilinear regime for $R \ll 1$ where we find anomalous transport; however, the quasilinear regime is still found,

including the particular dependence on the correlation lengths shown in Eq. (11), although shifted to larger values of R, $0.3 \lesssim R \lesssim 1$. The reason for which the quasilinear regime is obtained for $R \ll 1$ in the analytical studies, whereas we find it for $R \lesssim 1$, is because the system, in the analytical studies, is assumed to be stochastic from the start. However, the magnetic field line equations have an Hamiltonian structure such that the level of stochasticity (i.e., of chaos) is low for $R \ll 1$. In such a case closed magnetic surface, i.e., KAM tori, are found and anomalous transport results.

IV. DISCUSSION AND CONCLUSIONS

In this paper we have studied magnetic field line transport in 3D magnetic turbulence with anisotropy in the directions parallel and perpendicular to the magnetic field. Particular attention is devoted to the representation of the anisotropy, in order to assess its influence on the transport regimes. The main results of the present study are the following: We find that stochasticity increases both increasing the fluctuation level $\delta B/B_0$ and increasing the ratio $l_\parallel/l_\perp$ at fixed $\delta B/B_0$. It appears that the different transport regimes can be organized in terms of the Kubo number $R = (\delta B/B_0)(l_\parallel/l_\perp)$. When $R \ll 1$ weak chaos, closed magnetic surfaces, and anomalous transport regimes are found. When $R \gtrsim 0.3$ the diffusion regime is Gaussian, and the quasilinear scaling of the diffusion coefficient $D_\perp \sim (\delta B/B_0)^2$ is recovered for R up to 1. Finally, for $R \gg 1$ the percolation scaling of the diffusion coefficient $D_\perp \sim (\delta B/B_0)^{0.7}$ is obtained. These results are consistent with those of Zimbardo et al. and Pommois et al. [30,32], where the magnetic turbulence is isotropic and anomalous diffusion is found for $\delta B/B_0 \lesssim 0.2$. The percolation scaling of the diffusion coefficient was previously obtained in Refs. [5,29]. In particular, Reuss and Misguich [29] realized 2D simulations, to study particle diffusion in the guiding center approximation, and obtained the percolative scaling $\mu \sim 0.7$. Therefore this analytical limit is confirmed by the numerical results in the $l_\parallel/l_\perp \to \infty$ approximation.

It is interesting to note that a single parameter, the Kubo number $R = (\delta B/B_0)(l_\parallel/l_\perp)$, allows us to ''classify'' both the quasilinear and percolative regimes, and the level of stochasticity of the system. This unexpected result suggests that there is a relation between the Kubo number and the level of chaoticity of the system. In the problem of magnetic field line transport, the chaoticity is measured though the Kolmogorov entropy h [22,48], which corresponds to the largest Lyapunov exponent of field lines. A quasilinear estimate of the Kolmogorov entropy can be obtained as $h_{\rm ql} \simeq (\delta B/B_0)^2(l_\parallel/l_\perp^2)$ [22,30,48]. It is immediate to see that the Kolmogorov entropy can be expressed through the Kubo number as $h_{\rm ql} \simeq R^2/l_\parallel$. Therefore the Kubo number, originally defined as the parameter whose smallness allows a perturbative treament of a stochastic equation [27], is very directly related to the Kolmogorov entropy (or the Lyapunov exponents) of the system, and is an appropriate parameter to quantify the stochasticity of magnetic field lines. It would be interesting to investigate numerically the relation between h and R outside of the quasilinear regime and as a function of the degree of anisotropy.

ACKNOWLEDGMENTS

[1] B. B. Kadomtsev and O. P. Pogutse, in *Plasma Physics and Controlled Nuclear Fusion Research, Proceedings of the 7th International Conference*, Innsbruck, 1978 (IAEA, Vienna, 1979), Vol. 1, p. 649.

[2] J. A. Krommes, C. Oberman, and R. G. Kleva, J. Plasma Phys. **30**, 11 (1983).

[3] M. B. Isichenko, Plasma Phys. Controlled Fusion **33**, 795 (1991).

[4] M. B. Isichenko, Plasma Phys. Controlled Fusion **33**, 809 (1991).

[5] M. Ottaviani, Europhys. Lett. **20**, 111 (1992).

[6] P. C. Gray, D. H. Pontius, and W. H. Matthaeus, Geophys. Res. Lett. **23**, 965 (1996).

[7] M. Pettini, A. Vulpiani, J. H. Misguich, M. D. Leener, J. Orban, and R. Balescu, Phys. Rev. A **38**, 344 (1988).

[8] M. Vlad, F. Spineanu, J. H. Misguich, and R. Balescu, Phys. Rev. E **58**, 7359 (1998).

[9] W. H. Matthaeus, P. C. Gray, D. H. Pontius, Jr., and J. W. Bieber, Phys. Rev. Lett. **75**, 2136 (1995).

[10] W. H. Matthaeus, S. Oughton, S. Ghosh, and M. Hossain, Phys. Rev. Lett. **81**, 2056 (1998).

[11] P. Pommois, P. Veltri, and G. Zimbardo, Phys. Rev. E **59**, 2244 (1999).

[12] D. C. Robinson and M. G. Rusbrige, Phys. Fluids **14**, 2499 (1971).

[13] S. J. Zweben C. R. Menyuk, and R. J. Taylor, Phys. Rev. Lett. **42**, 1270 (1979).

[14] S. R. Spangler, Astrophys. J. **522**, 879 (1999).

[15] M. Dobrowolny, A. Mangeney, and P. Veltri, Astron. Astrophys. **83**, 26 (1980).

[16] M. Dobrowolny, A. Mangeney, and P. Veltri, Phys. Rev. Lett. **45**, 144 (1980).

[17] V. Carbone, F. Malara, and P. Veltri, J. Geophys. Res. **100**, 1763 (1995).

[18] G. Zimbardo and P. Veltri, Geophys. Res. Lett. **23**, 793 (1996).

[19] P. Veltri, G. Zimbardo, and P. Pommois, Adv. Space Res. **22**, 55 (1998).

[20] M. N. Rosenbluth, R. Z. Sagdeev, G. B. Taylor, and G. M. Zaslavsky, Nucl. Fusion **6**, 297 (1966).

[21] N. N. Filonenko R. Z. Sagdeev, and G. M. Zaslavsky, Nucl. Fusion **7**, 253 (1967).

[22] A. B. Rechester and M. N. Rosenbluth, Phys. Rev. Lett. **40**, 38 (1978).

[23] J. R. Jokipii, Astrophys. J. **146**, 480 (1966).

[24] J. R Jokipii and E. N. Parker, Phys. Rev. Lett. **21**, 44 (1968).

[25] J. R. Jokipii and E. N. Parker, Astrophys. J. **155**, 777 (1969).

[26] A. A. Galeev and L. M. Zelenyi, Physica D **2**, 90 (1981).

[27] R. Kubo, J. Math. Phys. **4**, 174 (1963).

[28] A. Brissaud and U. Frisch, J. Math. Phys. **15**, 524 (1974).

[29] J.-D. Reuss and J. H. Misguich, Phys. Rev. E **54**, 1857 (1996).

[30] G. Zimbardo, P. Veltri, G. Basile, and S. Principato, Phys. Plasmas **2**, 2653 (1995).

[31] G. Zimbardo and P. Veltri, Phys. Rev. E **51**, 1412 (1995).

[32] P. Pommois, G. Zimbardo, and P. Veltri, Phys. Plasmas **5**, 1288 (1998).

[33] M. Malavasi and N. Reggiani, in *Proceedings of the Magnetic Turbulence and Transport Workshop*, Cargèse, 1992, edited by P. Hennequin and M. A. Dubois (Editions de Physique, Orsay Les-Ullis, France, 1993), p. 49.

[34] A. Bazzani, A. M. Disebastiano, and G. Turchetti, Electromag. Waves Electron. **3**, 38 (1998).

[35] A. F. Barghouty and J. R. Jokipii, Astrophys. J. **470**, 858 (1996).

[36] S. Benkadda, P. Gabbai, and G. M. Zaslavsky, Phys. Plasmas **4**, 2864 (1997).

[37] J. Klafter, A. Blumen, and M. F. Shlesinger, Phys. Rev. A **35**, 3081 (1987).

[38] G. M. Zaslavsky, R. Z. Sagdeev, D. K. Chaikovsky, and A. A. Chernikov, Zh. Éksp. Teor. Fiz., **95**, 1723 (1989) [Sov. Phys. JETP **68**, 995 (1989)].

[39] X.-J. Wang, Phys. Rev. A **45**, 8407 (1992).

[40] J.-P. Bouchaud and A. Georges, Phys. Rep. **195**, 127 (1990).

[41] M. F. Shlesinger, B. J. West, and J. Klafter, Phys. Rev. Lett. **58**, 1100 (1987).

[42] J. Klafter, M. F. Shlesinger, and G. Zumofen, Phys. Today **49**, 33 (1996).

[43] G. M. Zaslavsky, D. Stevens, and H. Weitzner, Phys. Rev. E **48**, 1683 (1993).

[44] M. F. Shlesinger, G. M. Zaslavsky, and J. Klafter, Nature (London) **363**, 31 (1993).

[45] M. B.Isichenko, Rev. Mod. Phys. **64**, 961 (1992).

[46] P. Pommois, Ph.D. thesis, University of Calabria, Cosenza, Italy, 1998.

[47] R. H. Kraichnan, Phys. Fluids **8**, 1385 (1965).

[48] G. Zimbardo, P. Veltri, and F. Malara, J. Plasma Phys. **32**, 141 (1984).